water

MDPI

Article

Intensity-Duration-Frequency Curve for Extreme Rainfall Event Characterization, in the High Tropical Andes

Diego Escobar-González [1,*], Mélany S. Singaña-Chasi [2], Juan González-Vergara [3,4], Bolívar Erazo [1,5], Miguel Zambrano [6], Darwin Acosta [7], Marcos Villacís [8], Mario Guallpa [1], Braulio Lahuatte [3] and Diego H. Peluffo-Ordóñez [4,9,10]

1 Departamento de Gestión de Recursos Hídricos, Empresa Pública Metropolitana de Agua Potable y Saneamiento de Quito, EPMAPS Agua de Quito, Quito 170509, Ecuador
2 Ingeniería Civil, Facultad de Ingeniería y Ciencias Aplicadas, Universidad Central del Ecuador, Quito 170521, Ecuador
3 Fondo para la Protección del Agua, FONAG, Mariana de Jesús N32 y Martín de Utreras, Quito 170509, Ecuador
4 SDAS Research Group, Ben Guerir 43150, Morocco
5 Instituto Nacional de Meteorología e Hidrología, INAMHI, Iñaquito N36-14 y Corea, Quito 170507, Ecuador
6 Departamento de Ciencias Exactas, Universidad de las Fuerzas Armadas ESPE, Sangolquí 171103, Ecuador
7 Centro de Control Red Monitoreo Aire, Secretaría de Ambiente, Municipio del Distrito Metropolitano de Quito, Quito 170525, Ecuador
8 Departamento de Ingeniería Civil y Ambiental & Centro de Investigación y Estudios en Ingeniería de los Recursos Hídricos, Escuela Politécnica Nacional, Quito 170525, Ecuador
9 Modeling, Simulation and Data Analysis (MSDA) Research Program, Mohammed VI Polytechnic University, Lot 660, Hay Moulay Rachid, Ben Guerir 43150, Morocco
10 Faculty of Engineering, Corporación Universitaria Autónoma de Nariño, Carrera 28 No. 19-24, Pasto 520001, Colombia
* Correspondence: diego.p.escobar.g@gmail.com

check for updates

Citation: Escobar-González, D.; Singaña-Chasi, M.S.; González-Vergara, J.; Erazo, B.; Zambrano, M.; Acosta, D.; Villacís, M.; Guallpa, M.; Lahuatte, B.; Peluffo-Ordóñez, D.H. Intensity-Duration-Frequency Curve for Extreme Rainfall Event Characterization, in the High Tropical Andes. *Water* **2022**, *14*, 2998. https://doi.org/10.3390/w14192998

Academic Editor: Paul Kucera

Received: 15 July 2022
Accepted: 17 September 2022
Published: 23 September 2022

Publisher's Note: MDPI stays neutral with regard to jurisdictional claims in published maps and institutional affiliations.

Copyright: © 2022 by the authors. Licensee MDPI, Basel, Switzerland. This article is an open access article distributed under the terms and conditions of the Creative Commons Attribution (CC BY) license (https://creativecommons.org/licenses/by/4.0/).

Abstract: In fields such as hydrology, meteorology, and civil engineering, the study of extreme precipitation events is useful to prevent rainfall related disasters. A widely-used practice to address such a problem is by using statistical inferences about precipitation intensity, duration and frequency (IDF). Despite of its great usefulness, the selection of the adequate data and methodology to characterize precipitation's IDF in the urban area of high-altitude Andean cities remains an open issue for practitioners and decision makers. In this sense, the present paper develops an approach to schematically build the IDF curves for a sub-basin of the study case Andean city, Quito–Ecuador. The here-used data holds information from 12 meteorological stations. Then, the IDF curves are obtained by using both a parametrization followed by a Gamma distribution and a 3-parameter cumulative distribution function, also called *mnp*. Finally, the curve-fitting process is estimated numerically by adjusting the Sherman equation. Results (average $R^2 = 0.9$) demonstrated that the framework is well-suited for the high-altitude regime. As a noticeable outcome, a novel spatial interpolation-based analysis is introduced, which enabled the identification of extreme rainfall events according to its duration.

Keywords: Andean region; cumulative distribution function (CDF); IDF curves; rainfall intensity; rainfall zonification; Sherman equation

1. Introduction

Precipitation is one of the most relevant atmospheric variables for humans, for electrical energy generation, risk management, agriculture and planning of outdoor events. Every year, thousands of people are put at risk because of extreme weather events [1]. For example, floods can trigger infectious disease outbreaks and damage public and private infrastructure [1].

In general, when modeling extreme environmental events, like precipitation, it is often desired to understand their behavior over a region. In that matter, modeling the rainfall regime and knowing the distribution in the time span of intense storms serves of great purpose for designing and operating projects related to meteorology, hydrology, civil engineering, among others [2]. Therefore, practitioners around the world rely on Intensity-Duration-Frequency (IDF) curves, by using them as a graphical representation of the underlying mathematical relationship among precipitation intensity, its duration and observed frequency, for example [3–7]. Other studies have focused on developing IDF curves under different circumstances as climate change, heavy storms or urban applications [8–10]. Also, some works have studied the IDF curves using different types of information such as downscaled in situ data, daily and subdaily records and high resolution radar-based precipitation [11–13]. The use of IDF curves is so extensive that even in developing countries of South America, like Ecuador [14,15], they have become a key tool for decision makers [15–18].

Certainly, several studies have reported that Gumbel and Generalized Extremes Values distributions are commonly used, but none of the reviewed articles has explored the 3-parameter *mnp* methodology in South America. In this context, this work considers an approach to implement the IDF curves using a suitable cumulative distribution function (CDF) seen as the improvement of the Gamma probability function. The presented approach is based on the so-named 3-parameter *mnp* CDF introduced in [19–21] that allows to improve results associated to most extreme rainfall events, usually derived from the tail of density functions. As the standard *mnp* CDF has been used over the western Mediterranean area (in the low altitude city of Barcelona), the effort of the present study is to prove that it can also be fitted to the Andean conditions, in this case the high altitude mountain system of Quito, Ecuador.

To do so, the presented approach includes the following main 5 stages: (1) data cleaning and resizing, when needed; (2) maximum recorded rainfall events extraction; (3) selection of a statistical distribution for the maximum recorded rainfall events according to Akaike Information Criterion and the Bayesian Information Criterion; (4) IDF equations obtaining trough the Sherman equation and readjusting using the *mnp* CDF; and (5) plotting of the accumulated rainfall obtained by the IDF curves onto a spatial interpolation and several extreme precipitation events are discussed. Experiments were carried out over a high volume of information retrieved from Empresa Pública Metropolitana de Agua Potable y Saneamiento de Quito (`EPMAPS`) [22] and Secretaría de Ambiente del Distrito Metropolitano de Quito (`SADMQ`) [23] .

As remarkable results, meaningful insights and findings are accomplished by using the intensity values obtained from applying the *mnp* readjustment as the input to a novel spatial interpolation-based analysis to characterize rainfall intensity according to its duration. Furthermore, it is experimentally demonstrated that the obtained IDF equations are robust enough to properly describe extreme rainfall events representative of the Andean region.

The rest of the article is organized as follows. Section 2 describes the geographical and meteorological characteristics of the studied area. Section 3 presents the data used. Section 4 explains the data preprocessing techniques, the procedure for building IDF curves, the evaluation and the spatial interpolation technique. In Section 5, the yielded IDF curves and their error performance are presented. Additional results such as the processed data and interpolated maps are also shown. In Section 6, several extreme precipitation events are analyzed through the IDF curves. Finally, Section 7 states the conclusion and future works.

2. Study Area

Ecuador, due to its geographical position, has a very particular climate. The behavior of atmospheric weather in the country seems affected by the influence of the intertropical convergence zone. The Andes mountain range causes an interruption in the atmospheric circulation, resulting in a variety of mesoscale phenomena as well as very marked climatic conditions in short distances [24]. The geomorphology of the Metropolitan District of Quito

(DMQ) was formed in the Eocene when the sea withdrew, the Eastern Cordillera of the Andes began to appear and through orogenic movements folding, metamorphism and uplift of the mountain range were produced. At the same time erosive stages modeling landscapes were ongoing [25]. Subsequently, the Western Cordillera emerged, and erosive processes that have modeled the landscape throughout geological history took place [26]. The predominant geomorphology in Quito city is mountainous with volcanic reliefs, lava flows, plains of volcanic deposits and very high mountain reliefs [27].

The El Batán sub-basin, Figure 1, is located on the eastern flank of the Pichincha volcano, at coordinates 0°10′20.85″ S latitude and 78°29′59.68″ W longitude. For the present study 12 stations have been used, covering more than 56.06 km^2 contained in the study area.

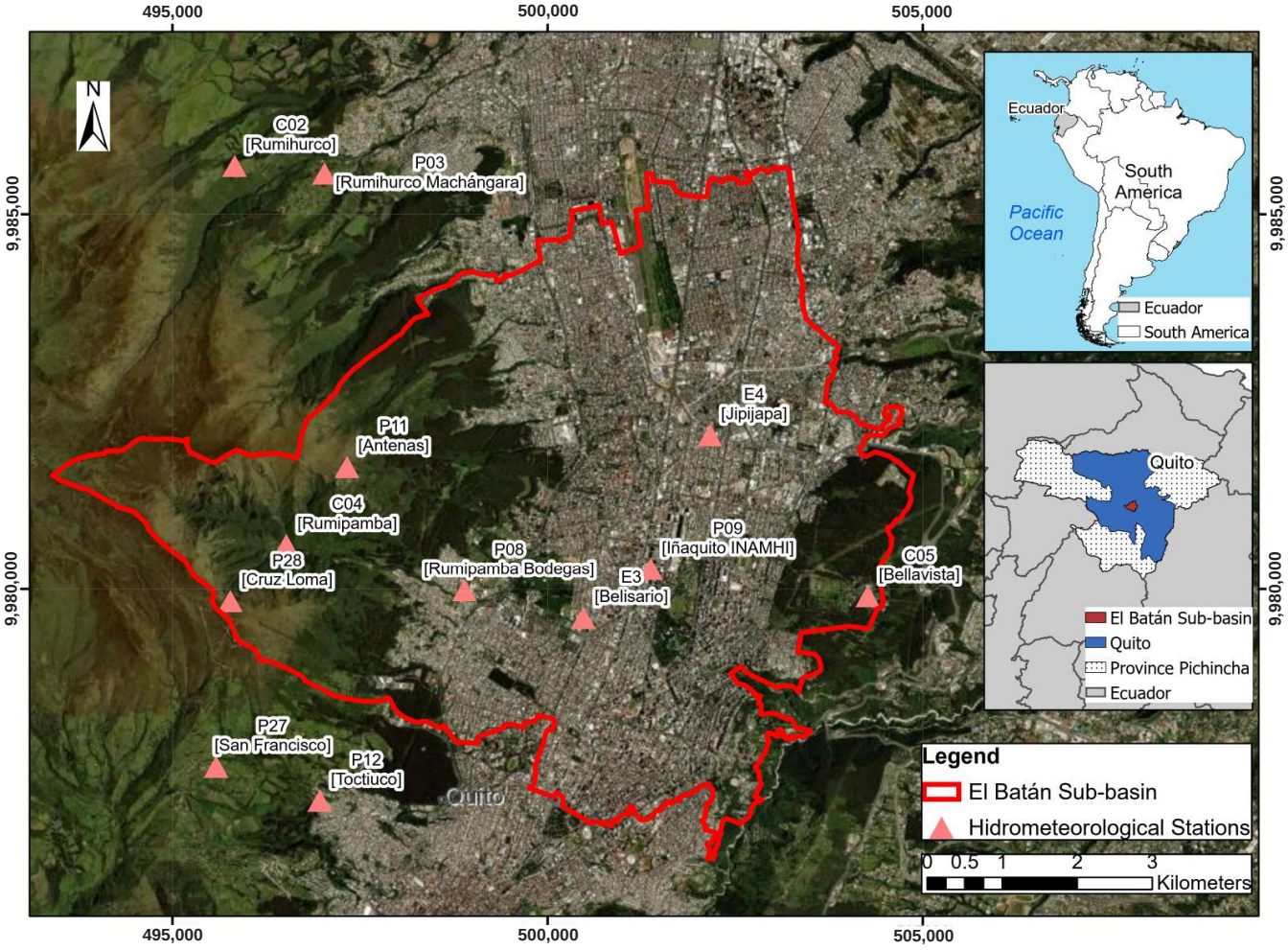

Figure 1. Topographical boundary of the study area: Quito-Ecuador, El Batán sub-basin.

The zone is mountainous with an average height of 3049.8 m above sea level (m.a.s.l.), in the high zone it reaches 4555 m.a.s.l. and in the lowest part of the city it oscillates between 2600 m.a.s.l. Furthermore, the temperature ranges between 1.5 and 22 degrees Celsius in the urban area of the basin. This sub-basin has 21.1% mean slope and is characterized by steep slopes. The average annual rainfall in the basin is 1185 mm, while the monthly average ranges between 25 and 175 mm, being April the wettest month with rainfall above 180 mm and August the driest month with just 25 mm. The average humidity of the sub-basin is 80%, with April being the wettest, and August the driest months, which is consistent with the bimodal distribution of rainfall, Figure 2.

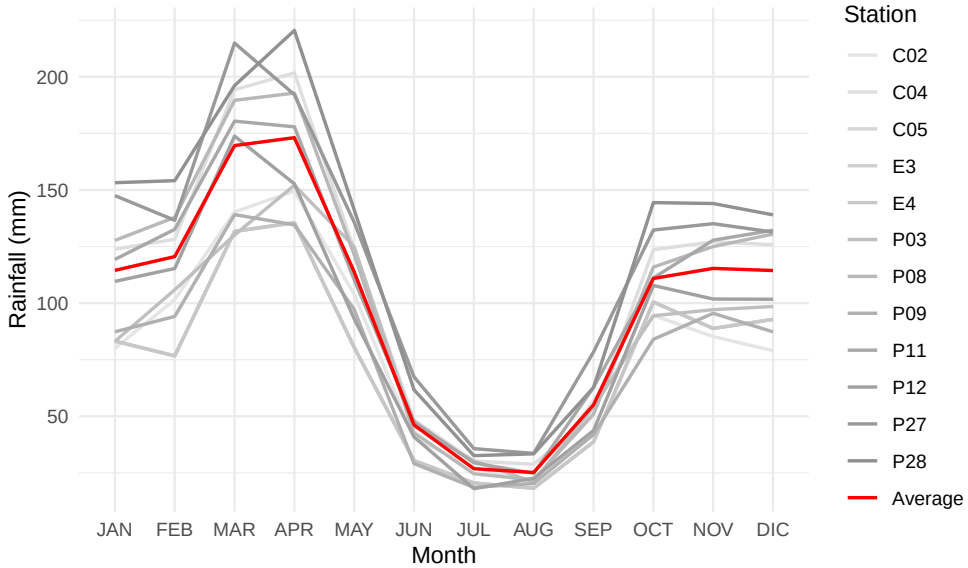

Figure 2. Multi-year monthly rainfall of each station (bluish) and Multi-year monthly mean rainfall (red) of El Batán sub-basin.

3. Data

Rainfall data density in Ecuador's capital, Quito, has increased over the last 20 years, thanks to the strengthening of local meteorological monitoring networks of Empresa Pública Metropolitana de Agua Potable y Saneamiento de Quito (`EPMAPS`) [22,28], Secretaría de Ambiente del Distrito Metropolitano de Quito (`SADMQ`) [23] and the already existing information of Instituto Nacional de Meteorología e Hidrología (`INAMHI`) [29]. Rainfall data was retrieved from two sources: `EPMAPS` (5-min timestamp) and `SADMQ`) (10-min timestamp). The latter undergoes a frequency reduction explained in Algorithm 1. Table 1 presents a general statistical overview of the datasets.

Table 1. Statistical description of raw data from `EPMAPS` and `SADMQ`, including the total amount of non-null samples, mean, standard deviation maximum values, and the the 99th percentile (PCTL) for values greater than zero.

Samples	P09	P11	P12	P03	C02	C05	P27	P28	P08	C04	E3	E4
Count	1,990,857	1,935,434	1,940,010	1,957,995	1,840,723	1,993,251	1,726,967	1,844,597	2,035,963	1,839,566	1,296,022	1,217,532
Mean	0.009	0.012	0.01	0.01	0.009	0.009	0.013	0.014	0.012	0.012	0.01	0.005
STD	0.093	0.101	0.104	0.095	0.087	0.094	0.114	0.103	0.113	0.109	0.109	0.06
99th PCTL	2.3	2.2	2.5	2.3	2	2.4	2.64	2	2.7	2.4	2.55	1.7
Max	10.3	7.6	8.6	10.1	7.1	9.7	10.2	8.64	9.12	9.1	10	8.2

Data Preprocessing

The preprocessing methodology aims at improving the quality of the data used to build the IDF curves and therefore its results. Accordingly, collected data was submitted to statistical validation and computational manipulation before being fed to the IDF curves. That is, extremely high isolated, inconsistent and negative records were deleted by identifying if their quantity could be possible given weather conditions at its time of capture [30]. Then, records where it was identified that the pluviometers received maintenance were removed. Finally, in order to have records with five minutes frequency in all samples, `SADMQ` data is downscaled. The process, detailed in Algorithm 1, is achieved by calculating the accumulated rainfall curve $\mathbf{P}$, from the rainfall time series $\mathbf{p} = (p_1, \ldots, p_i, \ldots, p_N)^\top$ with frequency of ten minutes as

$$\mathbf{P} = \left(p_1, \sum_{i=1}^{2} p_i, \sum_{i=1}^{3} p_i, \ldots, \sum_{i=1}^{N} p_i \right)^\top, \text{ where } P_N = \sum_{i=1}^{N} p_i. \tag{1}$$

Then, the intermediate accumulated rainfall $\mathbf{p}'$ and decumalating series $\mathbf{p}'$ is calculated as

$$\mathbf{P}' = \left(\frac{P_1}{2}, P_1, \frac{P_1 + P_2}{2}, P_2, \ldots, \frac{P_{N-1} + P_N}{2}, P_N \right)^\top, \tag{2}$$

$$\mathbf{p}' = \left(P'_1, \ldots, P'_{N-1} - P'_{N-2}, P'_N - P'_{N-1} \right)^\top, \tag{3}$$

Algorithm 1: Frequency reduction

1 **Input**: Rainfall time series $\mathbf{p} = (p_1, \ldots, p_i, \ldots, p_N)^\top$ with frequency of ten minutes.

1: From the original rainfall records, calculate the accumulated rainfall curve using Equation (1).
2: Calculate the average between consecutive records, as shown in Equation (2), and save it as the intermediate accumulated rainfall, which can be seen as a series of accumulated rainfall data with frequency of five minutes.
3: Decumulate the data and obtain a rainfall series every 5 min, using Equation (3).

Output: Rainfall time series $\mathbf{p}' = (p'_1, \ldots, p'_i, \ldots, p'_{2N})^\top$ with a frequency of five minutes.

Once a clean dataset is achieved, as suggested in [20], events of duration

$$\begin{aligned} \mathbf{D} &= (t_0, \ldots, t_d, \ldots, t_{25})^\top, \\ \mathbf{D} &= \mathbf{D}_1 \cup \mathbf{D}_2, \end{aligned} \tag{4}$$

are calculated, where $\mathbf{D}_1 = \{5, 10, 15, \ldots, 75\}$ min and $\mathbf{D}_2 = \{2, 4, 6, 9, 12, 14, 16, 18, 20, 22, 24\}$ h. As explained in Algorithm 2, given a rainfall time series $\mathbf{p} = (p_1, \ldots, p_j, \ldots, p_N)^\top$, each event is a rain episode temporarily separated from the rest by a lapse greater than the time interval under consideration t_d. That is, for a new event of duration t_d the accumulated rainfall is attractively calculated as:

$$acum = \sum_{step=j}^{step=j+d} p_{step} \tag{5}$$

and it is is counted as a unique event if it has the at least the same amount of consecutive zero values $(0\frac{\text{mm}}{\text{min}})$ of rainfall before the start of the next rainfall event, which is represented as

$$\sum_{step=j+1+d}^{step=j+1+d+d} p_{step} = 0.0. \tag{6}$$

In the case where two or more events are separated by a time shorter than the interval being studied, they are treated as two or more integral parts of a single event. This events and the maximum recorded data are used as the input for the following sections.

Algorithm 2: Sliding window algorithm for capturing maximum rainfall events

1 **Input**: Rainfall time series $\mathbf{p} = (p_1, \ldots, p_j, \ldots, p_N)^\top$ and the desired duration $\mathbf{D} = (t_0, \ldots, t_d, \ldots, t_{25})^\top$

1: Find rainfall values greater than zero as $start = p_j > 0.0$.
2: Calculate the accumulated rainfall of current event with Equation (5).
3: Calculate the separation with respect to following event using Equation (6).
4: While separation is not accomplished, store p_j as part of the event.
5: Find the maximum accumulated rainfall from each event.
6: Store the maximum accumulated rainfall for each duration t_d.

Output: Maximum rainfall events-

Figure 3, shows that events A (blue) and B (red) are both considered as single independent events of 50 min. Notice how the time interval separating each other is greater than the duration ($t_j = 50$ min) under consideration.

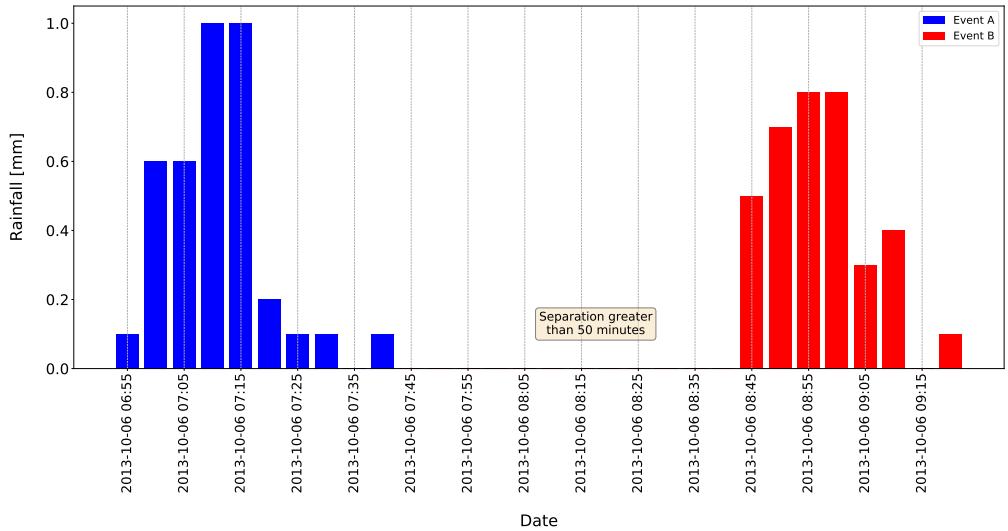

Figure 3. Example of two different events from station P28. Definitions and procedures from Algorithm 2 allows us to automatically capture events of different duration.

4. Methodology

The proposed methodology is presented as an alternative for building IDF curves in a high mountain ecosystem, Figure 4. The goal of this approach is to harness the statistical characteristics of grouped rainfall events to better generalize the IDF curves. At the same time, by using the *mnp* distribution, this approach seeks to yield better results for tailed data.

4.1. Distribution Functions and IDF Curves Construction

4.1.1. Statistical Distribution Selection and Parametrization

The best-fitted distribution function is selected through Akaike Information Criterion (AIC) [31] and the Bayesian Information Criterion (BIC) [32], by comparing the 28 distribution functions available in the R package `univariateML` [33].

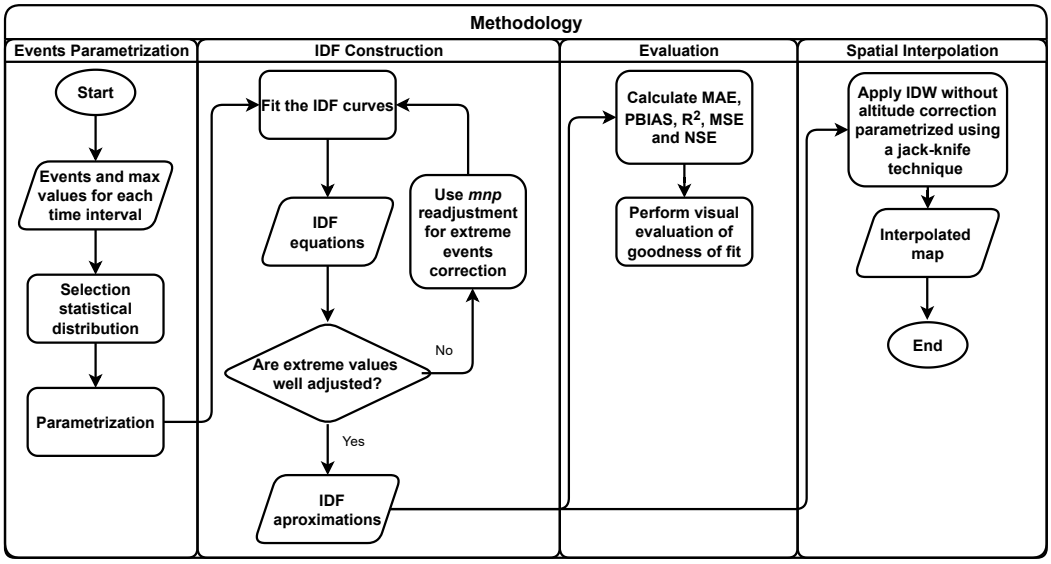

Figure 4. General overview of the methodolgy.

For each duration t_d, the time series of maximum recorded rainfall obtained from Algorithm 2 are used to calculate the CDF through the Gamma distribution. Then, In order to obtain the required parameters to fit the probability density function, the time series is fitted as:

$$f(x) = \begin{cases} \frac{\lambda(\lambda x)^{k-1}}{\Gamma(k)} e^{-\lambda x} & \text{if} \quad x \geq 0, \\ 0 & \text{otherwise}, \end{cases} \tag{7}$$

where the gamma function is

$$\Gamma(k) = \int_0^\infty t^{k-1} e^{-t} dt, \tag{8}$$

such that λ and k are the scale and shape parameters, both obtained from the mean m and the standard deviation σ, according to equations:

$$m = \frac{k}{\lambda}, \qquad \sigma^2 = \frac{k}{\lambda^2}. \tag{9}$$

Under those circumstances, the probability density function of the Gamma distribution is calculated as:

$$f(x) = \alpha x^\beta e^{-\lambda x}, \tag{10}$$

where

$$\alpha = \frac{P_{max} \lambda^k}{\Gamma(k)[1 + 3.32 \cdot \log_{10}(E)]}, \qquad \beta = k - 1, \qquad E = \text{number of events for each } t_d, \tag{11}$$

which are derived using the scale and shape parameter obtained from Equation (10) approximation.

4.1.2. IDF Fit

Considering each duration t_d and return periods $T = \{3, 5, 10, 15, 20, 25, 30, 50\}$ years, the CDF is solved for the rainfall amount (x), using the Newton-Raphson approximation of package [34] as:

$$\begin{aligned} T &= \frac{N}{E\Big(1 - F(x)\Big)}, \\ F(x) &= 1 - \frac{N}{TE}, \end{aligned} \tag{12}$$

where N is the number of years of information in each station.

Then, in order to obtain the IDF curves, the Sherman equation [35] is used as:

$$I(t_d) = \frac{a}{(t_d + b)^c}. \tag{13}$$

Following the approach in [20], parameter a has a logarithmic behavior with respect to the return period T, therefore a is rewritten as $a = ln(T) + B$. To finally obtain the IDF values, Equation (13) is fitted by solving the non-linear Equation (10) iteratively trough least squares method of [36] to find a, b, c.

4.1.3. The *mnp* Readjustment for Extreme Events Correction

IDF equations obtained from Section 4.1.1 underestimates values for short durations. To overcome such an issue, ref. [21] suggested using an adaptation of the Gamma probability, the so-called mnp CDF, Equation (14), taking into account only a data sample of return period greater than 1 year.

$$F(x) \approx G(x) = 1 - mx^n e^{-px}, \tag{14}$$

where the m, n, p coefficients are found by the least square method. At last, the definitive IDF curve is constructed by repeating Equation (13).

4.2. Evaluation

In order to evaluate the estimated maximum accumulated rainfall $\hat{p}_{max}(t_d)$ versus the maximum rainfall recorded $p_{max}(t_d)$ for a return period $T = 20$, the coefficients Mean Absolut Error (MAE), Root Mean Square Error (RMSE), Nash−Sutcliffe model efficiency coefficient (NSE), Mean Absolute Percentage Error (MAPE) and Pearson R^2 are calculated using [37]. The performance measures were chosen as suggested by [38,39].

Also, to grasp a visual idea of the goodness of fit obtained by the IDF curves, the maximum recorded rainfall for each t_d in $T = 20$ years is compared to the rainfall estimated by the IDF curves and the mnp approximation.

4.3. Interpolation

In order to analyze rainfall events from a spatial perspective, the accumulated rainfall data obtained from IDF curves of the 12 rain gauge stations was interpolated [40–43]. From these 26 rain-duration records, interpolation was performed using 1-km resolution raster datasets adapted to an effective regionalization protocol tested on poorly gauged regions and mountainous areas [40–43]. Selected method was Inverse Distance Weighting (IDW) without altitude correction, parametrized using a jack-knife technique [44] to select the exponent and gauge neighbors.

5. Results

Although the methodology was applied for all the stations, we have chosen to display detailed results for station P09—Iñaquito INAMHI (`EPMAPS`). In the case of frequency reduction, results for station E3-Belisario (`SADMQ`) are shown.

5.1. Data Preprocessing

Figure 5 displays the difference between raw and validated data. Frequency reduction process is shown in Figure 6. It can be observed that the rainfall storm behavior is not altered.

Captured events from station P09-Iñaquito INAMHI, are shown in Table 2.

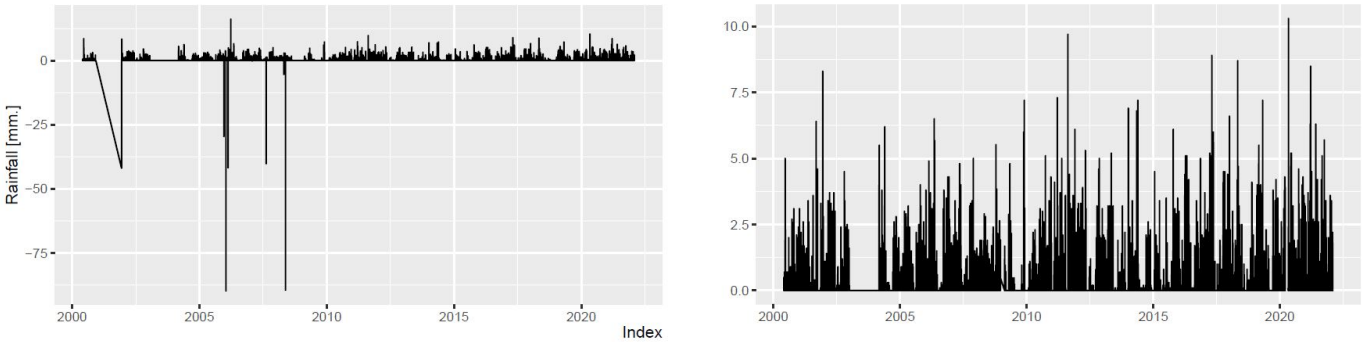

(**a**) Raw records. (**b**) Validated records.

Figure 5. Records before and after of data validation, Station P09. Extremely high isolated records were eliminated.

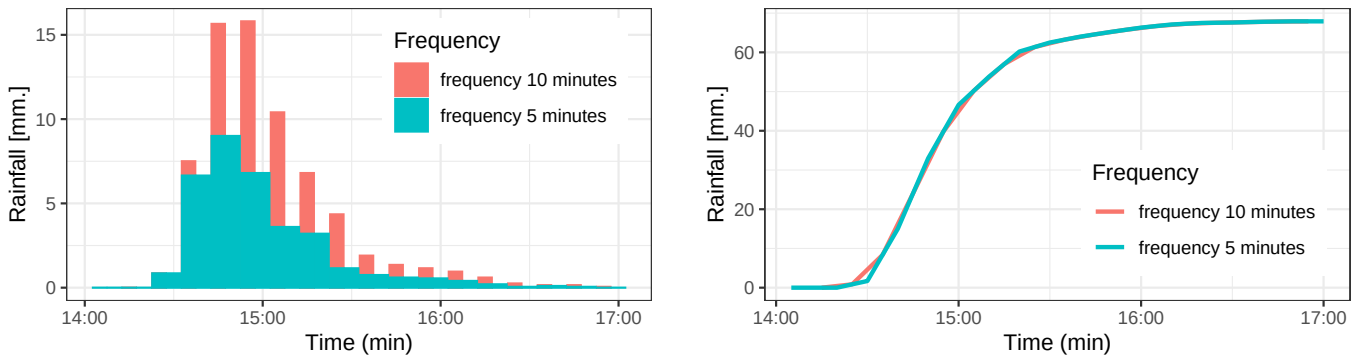

(**a**) Rainfall Records, Step 3 Algorithm 1 (**b**) Accumulated rainfall curve, Step 1 Algorithm 1

Figure 6. Example of frequency reduction from 10 to 5 min, in station Belisario SADMQ.

Table 2. Captured events: station P09-Iñaquito INAMHI.

Duration [min.]	E [Number of Events]	Max [mm.]	Mean [mm.]	Standard Deviation
5	20,470	10.3	0.2623	0.5336
10	14,106	20.2	0.4791	1.0667
15	11,536	27.3	0.6848	1.5079
20	10,073	31.6	0.8727	1.8778
25	9138	34.1	1.0394	2.1902
30	8443	35.6	1.1877	2.4603
35	7903	40.2	1.3212	2.6935
40	7498	42.8	1.4448	2.8962
45	7163	43.2	1.5534	3.0658
50	6907	43.4	1.6534	3.2138
55	6684	43.9	1.7424	3.3466
60	6425	44.3	1.8457	3.4829
65	6251	44.4	1.9286	3.5985
70	6095	44.5	2.0015	3.7012
75	5952	45.8	2.0713	3.7954
120	5025	60.8	2.6227	4.5085
240	3888	66.3	3.6254	5.6186
360	3289	66.4	4.3987	6.3900
540	2640	67.8	5.2310	7.2511
720	2164	73.9	6.0195	8.0285
840	1958	74	6.4143	8.4635
960	1778	74	6.7807	8.8716
1080	1624	74	7.1826	9.3408

Table 2. *Cont.*

Duration [min.]	E [Number of Events]	Max [mm.]	Mean [mm.]	Standard Deviation
1200	1511	74	7.5331	9.7840
1320	1365	74.1	8.1012	10.4412
1440	1230	74.3	8.8395	11.2411

5.2. Distribution Functions and IDF Curves Construction

5.2.1. Statistical distribution selection and parametrization

As expected from similar works [13], the strong theoretical foundations of BIC and AIC criterions to properly select statistical models are mirrored in Figure 7a,b. For each duration t_d, the best model is the one with the lowest values, that is the Gamma Inverse and Gamma Figure 7a,b.

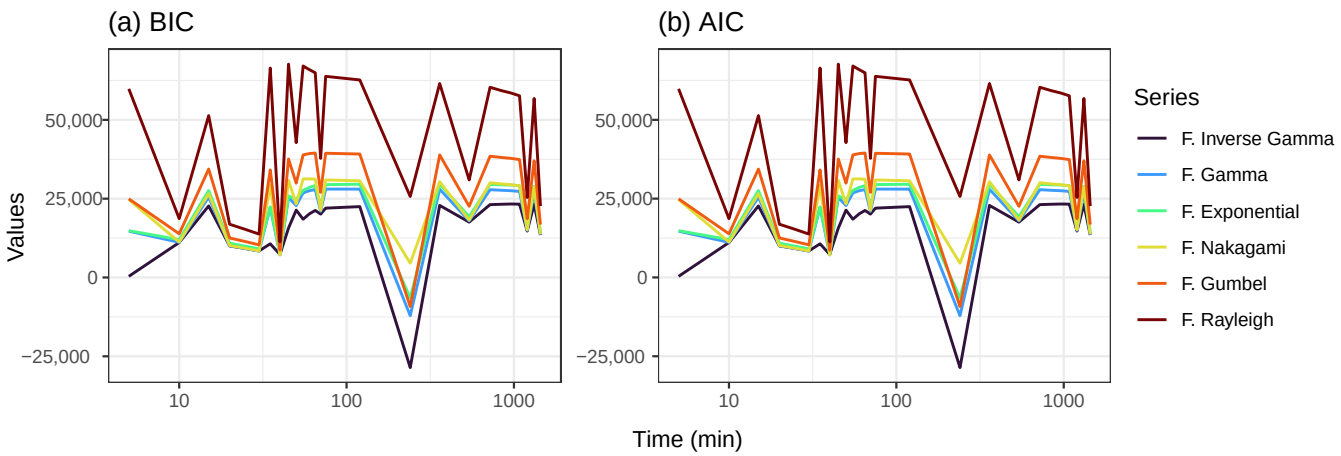

Figure 7. BIC and AIC information criteria of P28-Cruz Loma.

The values for the scale and shape parameters for each t_d are shown in Table 3.

Table 3. Fitting parameters of the Gamma distribution for every duration t_d.

Duration (min)	k	λ
5	0.2417	0.9213
10	0.2017	0.4211
15	0.2062	0.3012
20	0.2160	0.2475
25	0.2252	0.2167
30	0.2331	0.1962
35	0.2406	0.1821
40	0.2489	0.1723
45	0.2567	0.1653
50	0.2647	0.1601
55	0.2711	0.1556
60	0.2808	0.1521
65	0.2872	0.1489
70	0.2924	0.1461
75	0.2978	0.1438
120	0.3384	0.1290
240	0.4163	0.1148
360	0.4739	0.1077
540	0.5204	0.0995

Table 3. *Cont.*

Duration (min)	k	λ
720	0.5621	0.0934
840	0.5744	0.0895
960	0.5842	0.0862
1080	0.5913	0.0823
1200	0.5928	0.0787
1320	0.6020	0.0743
1440	0.6184	0.0700

5.2.2. IDF Fit & the *mnp* Readjustment for Extreme Events Correction

In Figure 8, an example of the resulting IDF curve for two return periods, obtained by applying the Gamma and *mnp* distribution is shown. The IDF curves are presented in Appendix A.1.

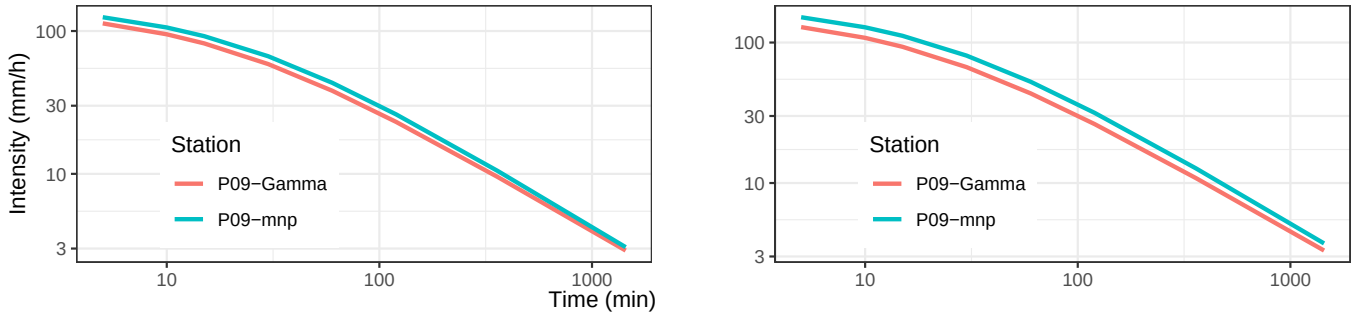

(**a**) 20 years Return Period (**b**) 50 years Return Period

Figure 8. Comparison of IDF curves fitting Gamma and *mnp* distribution.

5.3. Evaluation

Regarding the error metrics, Table 4 shows that:

$$\begin{aligned} &[1.95 < MAE < 6.99]\ \text{mm}, \quad \text{and} \quad \overline{MAE} = 3.36\ \text{mm}, \\ &[3.21 < RMSE < 9.12]\ \text{mm}, \quad \text{and} \quad \overline{RMSE} = 4.56\ \text{mm}. \end{aligned} \tag{15}$$

Thus, in the worst case $RMSE = 9.12$ mm, which is justified given that data is not normally distributed [45]. In general terms, both metrics suggest that the model is robust. Naturally, $\overline{MAE} \leq \overline{RMSE} \leq n^{\frac{1}{2}}$ holds. On the other according to [38], there is an excellent fit between simulations and observations, given that:

$$[0.84 < NSE < 0.98] \quad \text{and} \quad \overline{NSE} = 0.93. \tag{16}$$

Although, there might exist a slight underestimation of the IDF curves:

$$[0.0238 < MAPE < 0.1384]\% \quad \text{and} \quad \overline{MAPE} = 0.0592\%. \tag{17}$$

Furthermore, the average of the determination coefficient $\overline{R^2} = 0.96$ is considered. Notice that $R^2 > 0.9$ for all stations, pointing out that the proposed fit has a high degree of collinearity [38].

Table 4. Error metrics of the maximum recorded rainfall $p_{max}(t_d)$ recorded at different durations, with respect to the estimated rainfall $\hat{p}_{max}(t_d)$ of the IDF curves at $T = 20$ years.

Station Code	MAE	RMSE	NSE	MAPE	R^2
C02	2.8161	4.0359	0.9465	0.0336	0.9634
C04	2.1601	3.2093	0.9789	0.0580	0.9809
C05	4.0822	4.8267	0.9019	0.0240	0.9231
P03	3.7254	6.8351	0.8812	0.0325	0.9128
P08	1.9533	3.3155	0.9700	0.0238	0.9757
P09	2.9906	3.6563	0.9620	0.0502	0.9852
P11	2.2183	3.2757	0.9837	0.0548	0.9909
P12	6.9881	9.1153	0.8908	0.0724	0.9446
P27	2.6436	3.3288	0.9749	0.0279	0.9776
P28	3.6275	4.4120	0.9524	0.1384	0.9692
E3	3.8009	4.6277	0.9130	0.0889	0.9182
E4	3.3063	4.1126	0.8370	0.1060	0.9410
Average	3.3594	4.5626	0.9327	0.0592	0.9569

The visual evaluation of maximum recorded rainfall, IDF curve and *mnp* approximation for each t_d in $T = 20$ years, shows that in general there are not anomalies in the fit, Figure 9.

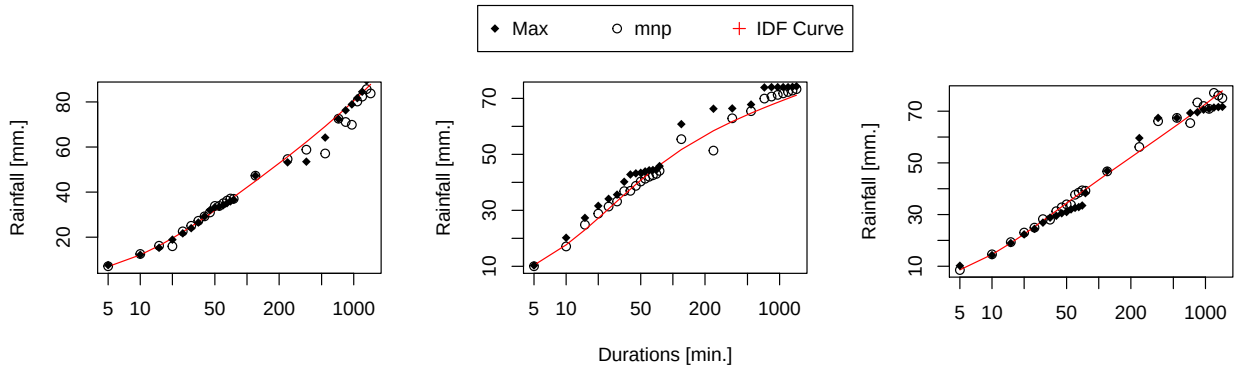

(**a**) P11-Antenas. (**b**) P09-Iñaquito INAMHI (**c**) P27-San Francisco

Figure 9. Maximum recorded rainfall at several t_d, accumulated rainfall obtained through *mnp* function and the estimated rainfall of the IDFs at $T = 20$ years.

5.4. Spatial Interpolation

Figure 10a shows that the greatest amount of rain occurs in the low altitude areas of the studied sub-basin, while in the high altitude zone the rainfall is less intense–Reinforcing the ideas explained in [42]. This pattern is repeated for events with durations $t_d \leq 120$ min. Additionally, it could be suggested that in the lower part of the basin, the generation of convective rainfall is more favorable, since events of shorter duration and greater intensity are more common.

In contrast, Figure 10b shows that the greatest amount of rainfall occurs in the higher altitude areas (close to 4000 m.a.s.l.) of the studied sub-basin, while in the lower areas the rainfall is as intense. This pattern is repeated for events with durations $t_d \geq 360$ min. Also, it could be suggested that in the high altitude zone of the basin, rainfall is formed trough contact between humidity and the surface. Additionally, at higher altitudes temperature decreases, favoring condensation and therefore low-intensity but long-lasting rain.

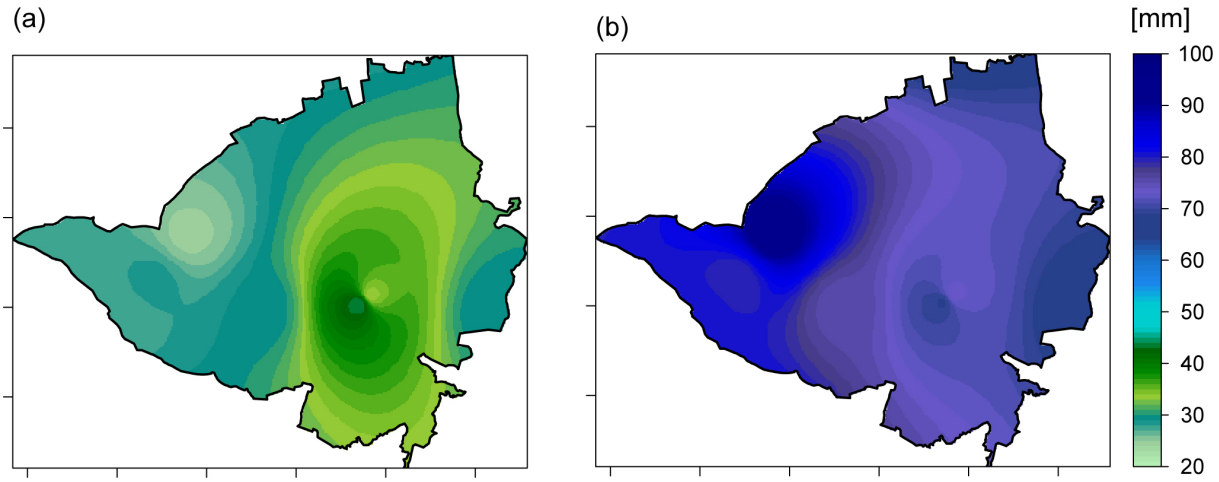

Figure 10. Spatial interpolation of rainfall events in El Batán Sub-basin (**a**) With duration $D = 30$ min and (**b**) With duration $D = 1440$ min and return period $T = 20$.

6. Discussion

The purpose of this study was to build the IDF curves for a sub-basin of the Andean city of Quito, Ecuador. Even though the *mnp* readjustment was first introduced in a low altitude area, the present study proved it well-suited to build the IDF of 12 rain gauged stations in a high-altitude region. The fact that it properly worked under very different conditions, makes it a high quality contender when choosing a methodology to build IDF curves. Therefore, in order to asses the methodology's scope, which could be replicated along the Andean region, the discussion is developed into three subsections. First, IDF curves are compared with local works developed in 2019 [15] and 1996 [14]. Then, using IDF curve as the main tool of analysis, two cases of extreme rainfall events are studied: a grade separation (underpass) flood that occurred in the north of Quito and a landslide in the neighborhood of La Gasca.

6.1. IDF Curves Comparison

Although there are many rain gauge stations to choose from, only P09—Iñaquito INAMHI (managed by `EPMAPS`) and M0024-INAMHI (managed by `INAMHI`) are shared among previous works. Nevertheless, this comparison makes the perfect fit since they are physically located in the same building.

In particular, Figure 11 shows that when analyzing short duration events, from 5 to 30 min, in $T = [5, 10, 20, 50]$ years, IDF's curves from this study resulted in lower intensity values compared to results performed in previous studies. For instance, an event of 120 mm/h in 5 min would have corresponded to $T = 5$ years, while using the here-obtained IDF curve, it would correspond to $T = 16.9$ years.

Additionally, statistics presented in Table 5 suggest that the equation obtained in this study is the best fit when compared to the previous studies.

Table 5. Error metrics of the maximum recorded rainfall $p_{max}(t_d)$ recorded at different durations, with respect to the estimated rainfall $\hat{p}_{max}(t_d)$ of the IDF curves at $T = 20$ years.

Station	MAE	RMSE	NSE	MAPE	R^2
P09-2022 [1]	2.9906	3.6563	0.9620	0.0502	0.9852
P09-1996 [2]	9.2461	14.1971	0.9049	0.1679	0.9343
M0024-2019 [3]	7.1453	9.7829	0.9548	0.1310	0.9600

Notes: [1] Results from this work. [2] Equation [14]. [3] Equation [15].

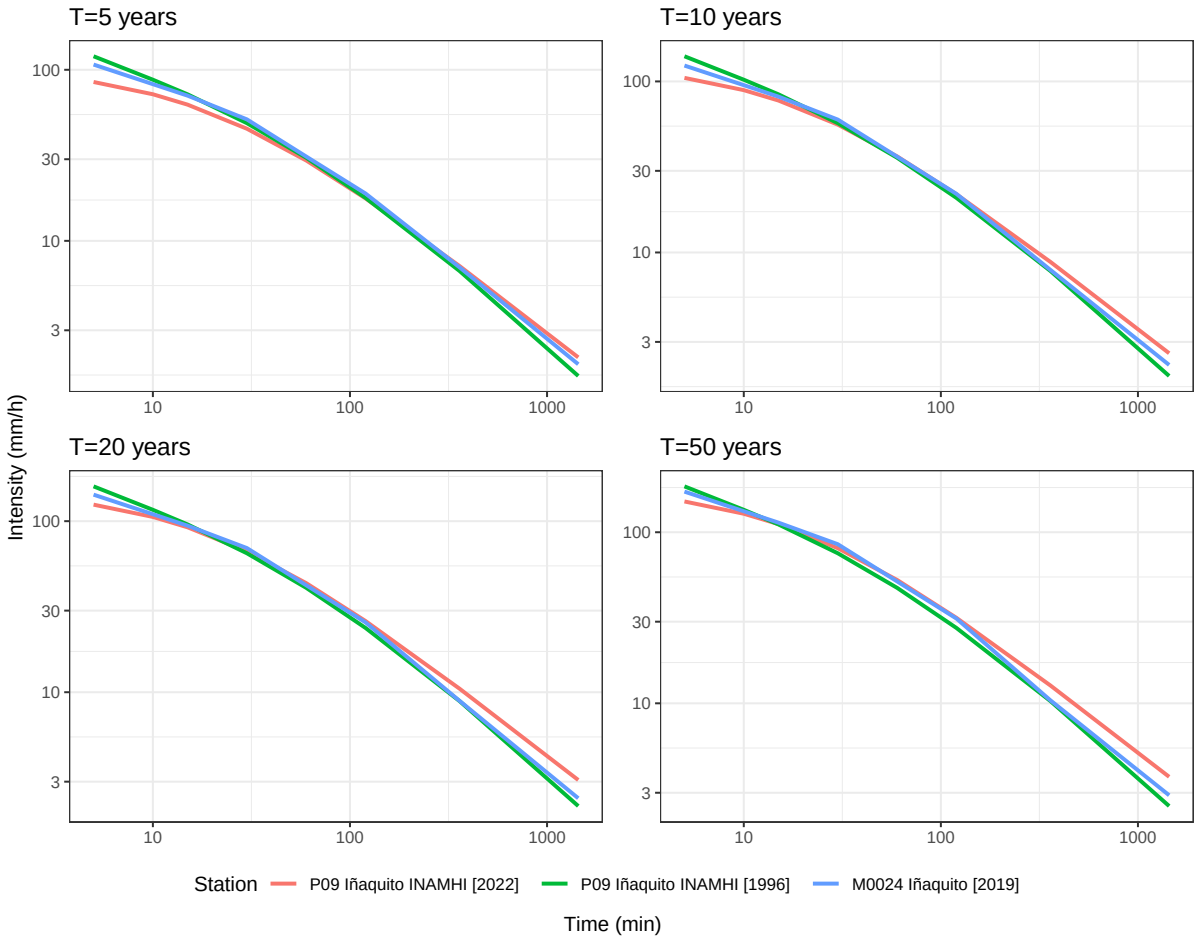

Figure 11. Comparisson of IDF curves, Iñaquito INAMHI.

6.2. Grade Separation (Underpass) Flood in the North of Quito

On 24 April 2017, an intense rainfall event generated the flooding of several grade separation structures, leaving vehicles trapped. The event was broadcasted by local media [46]. According to the hyetogram in Figure 12, first rainfall data was recorded by station E3 Belisario at 13h35 (UTC-5). Then, it extended to nearby stations that recorded information at approximately 1:45 p.m. The maximum recorded accumulated rainfall was 59 mm in 50 min. Figure 12 shows the consistency of the records since the hyetograms of the different stations have the same structure.

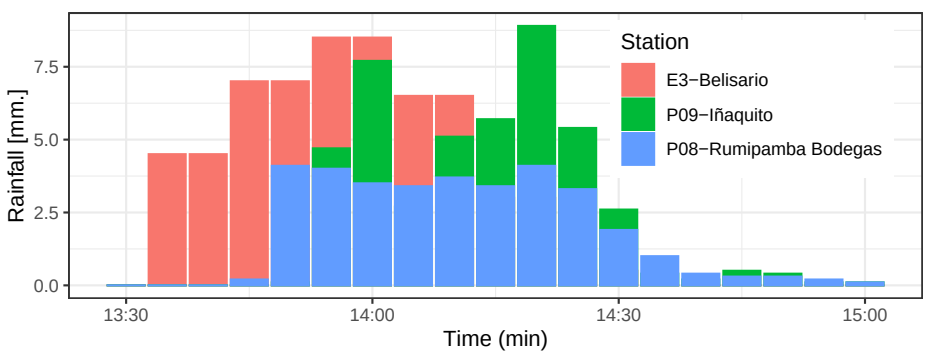

Figure 12. Hyetograms with 5-min record frequency of stations E3 Belisario, P08 Rumipamba Bodegas, P09 Iñaquito INAMHI, for the event of 24 April 2017.

According to IDF equation of E3 Belisario in Table A1, it corresponds to an event with $T = 25$ years. As expected, the recorded data clearly agrees with the IDF curves interpolation for all $t_d \leq 120$ min, Figure 10a. On the other hand, given the duration, it could be suggested that due to the amount of rain and intensity, it was produced by a deep convection event associated with a cloud of great vertical development type cumulonimbus [47].

6.3. La Gasca Lanslide

Obtained results allowed us to characterize events such as the so-called "Aluvión de La Gasca", which occurred on 31 January 2022, which was widely covered by the press [48–50]. In particular, station P28 Cruz Loma located within the study sub-basin, in the upper zone accumulated 75.1 mm in approximately 22 h of continuous rain.

According to Table A1, the equation for station P28 Cruz Loma, such rainfall corresponds to an event with a return period of approximately 16 years. As expected, the recorded data clearly agrees with the IDF curves interpolation for all $t_d \geq 360$ min, Figure 10b. In general, this event might be associated with mesoscale convective systems (MCSs), characterized by highly variable intensity and several hours of duration.

7. Conclusions

In this study, rainfall has been modeled trough mathematical functions relating its intensity, duration and frequency of occurrence (IDF curves). It has been proved that using the Gamma distribution function, the Sherman equation and the mnp CDF readjustment for extreme precipitation events is of great usefulness in a high-altitude sub-basin characterization. The obtained IDF curves exhibited robustness among error metrics as well as a high degree of collinearity, outperforming previous works. Equally important, by using the obtained IDF equations as the main tool of analysis, several extreme rainfall events were successfully explained. Likewise, by using the rainfall approximation obtained by the IDF equations, a novel spatial interpolation-based analysis enabled a better understanding of the distribution of rainfall at different altitudes according to its duration. A variety of future works might emerge from this study. For instance, captured rainfall events could lead to cluster analysis and data-based forecasting models, meanwhile IDF curves are key to hyetographs, design storms, climate change analysis and even prevention of rainfall related disasters.

Author Contributions: D.E.-G.: conceptualization, data curation, formal analysis, investigation, funding acquisition, methodology, project administration, supervision; M.S.S.-C.: investigation, methodology, and software; J.G.-V.; software, validation, interpretation of data, writing-original draft, project administration; B.E.: methodology, discussion formal analysis; M.Z.: software, review draft preparation; D.A., M.V., M.G. and B.L.: review draft preparation, D.H.P.-O.: writing—review & editing. All authors have read and agreed to the published version of the manuscript.

Funding: The authors gratefully acknowledge "Estación Científica Agua y Páramo" (ECAP).

Institutional Review Board Statement: Not applicable.

Data Availability Statement: Please refer to EPMAPS: pronostico.lluvias@aguaquito.gob.ec, Secretaría de Ambiente: darwin.acosta@quito.gob.ec.

Acknowledgments: This research project has been coordinated and directed with the help of Departamento de Gestión de Recursos Hídricos-Unidad de Hidrología of EPMAPS, ECAP and FONAG, to whiches all authors kindly thank. Also, authors appreciate the participation of SADMQ and SDAS Research Group.

Conflicts of Interest: The authors declare no conflict of interest.

Abbreviations

The following abbreviations are used in this manuscript:

Term	Description
EPMAPS	Empresa Pública Metropolitana de Agua Potable y Saneamiento del Distrito Metropolitano de Quito
SADMQ	Secretaría de Ambiente del Distrito Metropolitano de Quito
ECAP	Estación Científica Agua y Páramo
FONAG	Fondo para la Protección del Agua
AIC	Akaike Information Criterion
BIC	Bayesian Information Criterion
IDF	Intensity-Duration-Frequency
IDW	Inverse Distance Weighting
MAE	Mean Absolute Error
MAPE	Mean Absolute Percentage Error
RMSE	Root Mean Square Error
NSE	Nash-Sutcliffe model efficiency coefficient
PBIAS	Percent Bias

Appendix A

Appendix A.1

Table A1. IDF Equations for stations located in El Batán Sub-basin.

Station Name	Code	Institution	IDF Equation (mm/min)
Rumihurco	C02	EPMAPS	$I(t,T) = \frac{3.4156 \ln T + 12.3366}{(23.2947+t)^{0.8458}}$
Rumipamba	C04	EPMAPS	$I(t,T) = \frac{2.3179 \ln T + 12.8988}{(13.1224+t)^{0.8090}}$
Bellavista	C05	EPMAPS	$I(t,T) = \frac{3.4788 \ln T + 17.9663}{(16.7382+t)^{0.8795}}$
Rumihurco Machángara	P03	EPMAPS	$I(t,T) = \frac{5.3159 \ln T + 12.0554}{(18.7983+t)^{0.8618}}$
Rumipamba Bodegas	P08	EPMAPS	$I(t,T) = \frac{2.9057 \ln T + 17.6075}{(17.7225+t)^{0.8538}}$
Iñaquito INAMHI	P09	EPMAPS	$I(t,T) = \frac{9.1731 \ln T + 12.1785}{(20.2066+t)^{0.9132}}$
Antenas	P11	EPMAPS	$I(t,T) = \frac{1.8188 \ln T + 10.3480}{(19.7550+t)^{0.7558}}$
Toctiuco	P12	EPMAPS	$I(t,T) = \frac{1.9449 \ln T + 10.3656}{(6.4219+t)^{0.7755}}$
San Francisco	P27	EPMAPS	$I(t,T) = \frac{2.9177 \ln T + 14.8268}{(17.8184+t)^{0.8362}}$
Cruz Loma	P28	EPMAPS	$I(t,T) = \frac{6.6483 \ln T + 6.2078}{(23.6418+t)^{0.8430}}$
Belisario	E3	SADMQ	$I(t,T) = \frac{14.4305 \ln T + 17.0133}{(14.3124+t)^{0.9802}}$
Jipijapa	E4	SADMQ	$I(t,T) = \frac{9.7766 \ln T + 11.7882}{(23.9857+t)^{0.9639}}$

Appendix A.2

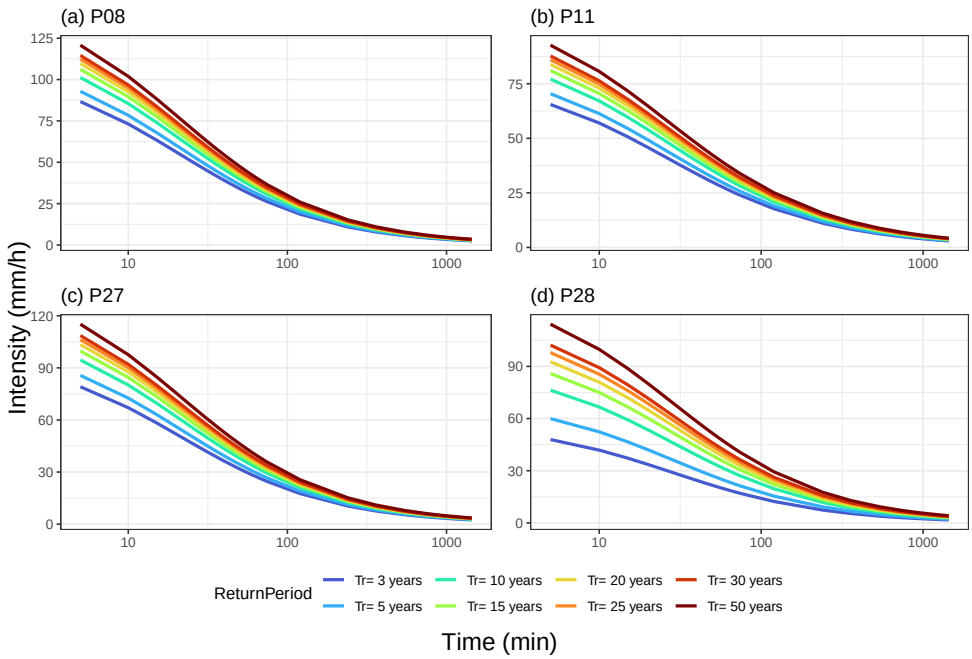

Figure A1. IDF Curves.

References

1. WHO. *Atlas of Health and Climate*; E-Book:WHO Press, World Health Organization (WHO): Geneva, Switzerland, 2012. Available online: https://www.who.int/publications/i/item/9789241564526 (accessed on 16 September 2022).
2. Pelosi, A.; Furcolo, P.; Rossi, F.; Villani, P. The characterization of extraordinary extreme events (EEEs) for the assessment of design rainfall depths with high return periods. *Hydrol. Process.* **2020**, *34*, 2543–2559. [CrossRef]
3. Mohymont, B.; Demarée, G.R.; Faka, D.N. Establishment of IDF-curves for precipitation in the tropical area of Central Africa—Comparison of techniques and results. *Nat. Hazards Earth Syst. Sci.* **2004**, *4*, 375–387. doi: 10.5194/nhess-4-375-2004. [CrossRef]
4. Al-Amri, N.S.; Subyani, A.M. Generation of Rainfall Intensity Duration Frequency (IDF) Curves for Ungauged Sites in Arid Region. *Earth Syst. Environ.* **2017**, *1*, 8. doi: 10.1007/s41748-017-0008-8. [CrossRef]
5. Wagesho, N.; Claire, M. Analysis of rainfall intensity-duration-frequency relationship for Rwanda. *J. Water Resour. Prot.* **2016**, *8*, 706. [CrossRef]
6. Minh, H.V.T.; Lavane, K.; Lanh, L.T.; Thinh, L.V.; Cong, N.P.; Ty, T.V.; Downes, N.K.; Kumar, P. Developing Intensity-Duration-Frequency (IDF) Curves Based on Rainfall Cumulative Distribution Frequency (CDF) for Can Tho City, Vietnam. *Earth* **2022**, *3*, 866–880. doi: 10.3390/earth3030050. [CrossRef]
7. Kareem, D.A.; M Amen, A.R.; Mustafa, A.; Yüce, M.I.; Szydłowski, M. Comparative Analysis of Developed Rainfall Intensity–Duration–Frequency Curves for Erbil with Other Iraqi Urban Areas. *Water* **2022**, *14*, 419. [CrossRef]
8. Shrestha, A.; Babel, M.S.; Weesakul, S.; Vojinovic, Z. Developing Intensity–Duration–Frequency (IDF) curves under climate change uncertainty: The case of Bangkok, Thailand. *Water* **2017**, *9*, 145. [CrossRef]
9. Huff, F.A. Time distribution of rainfall in heavy storms. *Water Resour. Res.* **1967**, *3*, 1007–1019. [CrossRef]
10. Balbastre-Soldevila, R.; García-Bartual, R.; Andrés-Doménech, I. A Comparison of Design Storms for Urban Drainage System Applications. *Water* **2019**, *11*, 757. doi: 10.3390/w11040757. [CrossRef]
11. Sun, Y.; Wendi, D.; Kim, D.E.; Liong, S.Y. Deriving intensity–duration–frequency (IDF) curves using downscaled in situ rainfall assimilated with remote sensing data. *Geosci. Lett.* **2019**, *6*, 17. [CrossRef]
12. Kawara, A.Q.; Elsebaie, I.H. Development of Rainfall Intensity, Duration and Frequency Relationship on a Daily and Sub-Daily Basis (Case Study: Yalamlam Area, Saudi Arabia). *Water* **2022**, *14*, 897. doi: 10.3390/w14060897. [CrossRef]
13. Ghebreyesus, D.T.; Sharif, H.O. Development and Assessment of High-Resolution Radar-Based Precipitation Intensity-Duration-Curve (IDF) Curves for the State of Texas. *Remote Sens.* **2021**, *13*, 2890. doi: 10.3390/rs13152890. [CrossRef]
14. Ayabaca, E.; Cruz, F.; Gutiérrez, C. *Curvas Intensidad-Duración-Frecuencia de Principales Estaciones Pluviográficas de Quito*; Technical Report; EMAAP-Quito: Quito, Ecuador, 1996.
15. INAMHI. *Determinación de Ecuaciones para el Cálculo de Intensidades Máximas de Precipitación*; Technical Report; Instituto Nacional Meteorológico e Hidrológico: Quito, Ecuador, 2019.
16. Zevallos, J.; Gutiérrez, R.; Lavado, W. *Generación de Curvas Intensidad-Duración-Frecuencia en Perú*; Pontificia Universidad Católica del Perú Tesis Lima: Perú, Ecuador, 2019.

17. Jove, F.; Hernández, R.; Caballero, A. IDF Curves and Maximum Rainfall in 24 hours in the Subregions of La Mojana and San Jorge in Northern Colombia. *Int. J. Eng. Res. Technol.* **2020**, *13*, 2884–2894. doi: 10.37624/IJERT/13.10.2020.2884-2894. [CrossRef]
18. Bertoni, J.C.; Martínez, F.M.G.; Brarda, J.P.; Tibaldo, O.; Rudolf, C.; Verga, L. Actualización de Relaciones Iintensidad-Duración-Frecuencia (IDF) de la Ciudad de Rafaela (Provincia de Santa Fe, Argentina). *II Taller Sobre Reg. Precipitaciones Máximas* **2009**, *2*, 8.
19. Casas, M.C.; Codina, B.; Redaño, A.; Lorente, J. A methodology to classify extreme rainfall events in the western Mediterranean area. *Theor. Appl. Climatol.* **2004**, *77*, 139–150. [CrossRef]
20. Casas Castillo, M.C. Análisis Espacial y Temporal de las Lluvias Extremas en Catalunya. Modelización y Clasificación Objetiva. Ph.D. Thesis, Departament d'Astronomia i Meteorologia, Universidad de Barcelona, Barcelona, Spain, 2005.
21. Navarro Bosque, J. Organització Espacial i Temporal de la Pluja a L'àrea Metropolitana de Barcelona. Ph.D. Thesis, Universitat Politècnica de Catalunya, Barcelona, Spain, 2022.
22. EPMAPS. Empresa Pública Metropolitana de Agua Potable Y Saneamiento. 2022. Available online: https://www.aguaquito.gob.ec/ (accessed on 16 September 2022).
23. SADMQ. Secretaría de Ambiente del Distrito Metropolitano de Quito. 2022. Available online: www.quitoambiente.gob.ec (accessed on 16 September 2022).
24. Garreaud, R.D. The Andes climate and weather. *Adv. Geosci.* **2009**, *22*, 3–11. [CrossRef]
25. Marocco, R.; Winter, T. *Capítulo 2-Bosquejo de la Evolución Geodinámica del Ecuador*; Centro Ecuatoriano de Investigación Geográfica: Quito, Ecuador, 1997.
26. Boschman, L.M. Andean mountain building since the Late Cretaceous: A paleoelevation reconstruction. *Earth-Sci. Rev.* **2021**, *220*, 103640. doi: doi: 10.1016/j.earscirev.2021.103640. [CrossRef]
27. Perrin, J.L.; Sierra, A.; Fourcade, B.; Poulenard, J.; Risser, V.; Janeau, J.L.; Gueguen, P.; Hubert, S. Quito Face a un Risque D'origine Naturelle la lave Torrentielle du 31 Mars 1997 dans le Quartier de la Comuna. Programme SISHILAD, EMAAP-Q, INAMHI, ORSTOM. 1997. Available online: https://www.researchgate.net/publication/32969940_Quito_face_a_un_risque_d%27origine_naturelle_la_lave_torrentielle_du_31_mars_1997_dans_le_quartier_de_La_Comuna (accessed on 16 September 2022).
28. Quito-Informa. Epmaps Cuenta con la Red Hidrometeorológica Más Completa del país. 2022. Available online: http://www.quitoinforma.gob.ec/2022/05/19/epmaps-cuenta-con-la-red-hidrometeorologica-mas-completa-del-pais/ (accessed on 16 September 2022).
29. SADMQ. Instituto Nacional de Meteorología e Hidrología. 2022. Available online: https://www.inamhi.gob.ec/ (accessed on 16 September 2022).
30. Lana, X.; Rodríguez-Solà, R.; Martínez, M.; Casas-Castillo, M.; Serra, C.; Burgueño, A. Characterization of standardized heavy rainfall profiles for Barcelona city: Clustering, rain amounts and intensity peaks. *Theor. Appl. Climatol.* **2020**, *142*, 255–268. [CrossRef]
31. Akaike, H. A new look at the statistical model identification. *IEEE Trans. Autom. Control* **1974**, *19*, 716–723. [CrossRef]
32. Schwarz, G. Estimating the dimension of a model. *Ann. Stat.* **1978**, *6*, 461–464. [CrossRef]
33. Moss, J. univariateML: An R package for maximum likelihood estimation of univariate densities. *J. Open Source Softw.* **2019**, *4*, 1863. [CrossRef]
34. Borchers, H.W.; Borchers, M.H.W. Package "Pracma". 2022. Available online: https://mirror.las.iastate.edu/CRAN/web/packages/pracma/pracma.pdf (accessed on 16 September 2022).
35. Sherman, C.W. Frequency and intensity of excessive rainfalls at Boston, Massachusetts. *Trans. Am. Soc. Civ. Eng.* **1931**, *95*, 951–960. [CrossRef]
36. Team, R.C.; Team, M.R.C.; Suggests, M.; Matrix, S. Package "Stats". In *The R Stats Package*; R Foundation for Statistical Computing: Vienna, Austria, 2018.
37. Zambrano-Bigiarini, M. *hydroGOF: Goodness-of-Fit Functions for Comparison of Simulated and Observed Hydrological Time Series*; R Package Version 0.4-0; Zenodo, 2020. doi: 10.5281/zenodo.839854. [CrossRef]
38. Moriasi, D.N.; Gitau, M.W.; Pai, N.; Daggupati, P. Hydrologic and water quality models: Performance measures and evaluation criteria. *Trans. ASABE* **2015**, *58*, 1763–1785.
39. De Myttenaere, A.; Golden, B.; Le Grand, B.; Rossi, F. Mean absolute percentage error for regression models. *Neurocomputing* **2016**, *192*, 38–48. [CrossRef]
40. Erazo, B.; Bourrel, L.; Frappart, F.; Chimborazo, O.; Labat, D.; Dominguez-Granda, L.; Matamoros, D.; Mejia, R. Validation of satellite estimates (Tropical Rainfall Measuring Mission, TRMM) for rainfall variability over the Pacific slope and Coast of Ecuador. *Water* **2018**, *10*, 213. [CrossRef]
41. Ruelland, D. Should altitudinal gradients of temperature and precipitation inputs be inferred from key parameters in snow-hydrological models? *Hydrol. Earth Syst. Sci.* **2020**, *24*, 2609–2632. [CrossRef]
42. Erazo, B. Representing Past and Future Hydro-Climatic Variability over Multi-Decadal Periods in Poorly-Gauged Regions: The Case of Ecuador. Ph.D. Thesis, Université Paul Sabatier-Toulouse III, Toulouse, France, 2020.
43. González-Zeas, D.; Erazo, B.; Lloret, P.; De Bièvre, B.; Steinschneider, S.; Dangles, O. Linking global climate change to local water availability: Limitations and prospects for a tropical mountain watershed. *Sci. Total Environ.* **2019**, *650*, 2577–2586. [CrossRef]
44. Brath, A.; Castellarin, A.; Montanari, A. Assessing the reliability of regional depth-duration-frequency equations for gaged and ungaged sites. *Water Resour. Res.* **2003**, *39* , 1367. [CrossRef]

45. Hodson, T.O. Root mean square error (RMSE) or mean absolute error (MAE): When to use them or not. *Geosci. Model Dev. Discuss.* **2022**, *15*, 5481–5487. [CrossRef]
46. Un Aguacero Anega las Calles de Quito. 2017. Available online: https://www.elcomercio.com/actualidad/quito/quito-lluvias-inundacion-emergencias-coe.html (accessed on 16 September 2022).
47. Bader, M.; Forbes, G.; Grant, J.; Lilley, R.; Waters, A. *Images in Weather Forecasting. A Practical Guide for Interpreting Satellite and Radar Imagery*; Cambridge University Press: Cambridge, UK, 1995.
48. Ecuador: Deadly Landslide after Heaviest Rainfall in Years. 2022. Available online: www.bbc.com/news/world-latin-america-60211539 (accessed on 16 September 2022).
49. Regen Verursacht Katastrophe in Quito. 2022. Available online: https://p.dw.com/p/46OY9 (accessed on 16 September 2022).
50. Léa Hurel, Ecuador: Comienza en Quito la Remoción de Escombros tras el Aluvión que dejó Decenas de Muertos. 2022. Available online: https://www.france24.com/es/am%C3%A9rica-latina/20220204-ecuador-aluvion-quito-lluvias-remocion (accessed on 16 September 2022).